GLIA

Pyruvate dehydrogenase kinase 2 knockdown restores the ability of ALS-linked SOD1G93A rat astrocytes to support motor neuron survival by increasing mitochondrial respiration

Journal:	*GLIA*
Manuscript ID	GLIA-00233-2022.R1
Wiley - Manuscript type:	Research Article (Direct Via EEO)
Date Submitted by the Author:	28-Dec-2023
Complete List of Authors:	Miquel, Ernesto; Universidad de la República Facultad de Medicina, Departamento de Histología y Embriología Villarino, Rosalía; Universidad de la República Facultad de Medicina, Departamento de Histología y Embriología Martínez-Palma, Laura; Universidad de la República Facultad de Medicina, Departamento de Histología y Embriología Cassina, Adriana; Universidad de la República Facultad de Medicina, Departamento de Bioquímica; Universidad de la República Facultad de Medicina, Centro de Investigaciones Biomédicas (CEINBIO) Cassina, Patricia; Universidad de la República Facultad de Medicina, Departamento de Histología y Embriología
Topics:	Astrocytes, Neurodegenerative diseases, Metabolic interactions with neurons
Techniques:	Immunocytochemistry, Cell culture techniques, PCR, Reducing gene expression in the brain via antisense methods, Analysis of brain metabolism
Keywords:	PDK2, Astrocytes, Mitochondria, ALS

Title page:

Pyruvate dehydrogenase kinase 2 knockdown restores the ability of ALS-linked SOD1G93A rat astrocytes to support motor neuron survival by increasing mitochondrial respiration

1) Ernesto Miquel: miquel@fmed.edu.uy / ernestomiquel@gmail.com
Departamento de Histología y Embriología, Facultad de Medicina, Universidad de la República. Av. Gral. Flores 2125. 11800, Montevideo, Uruguay
2) Rosalía Villarino: rosalia.villarino.m@gmail.com
Departamento de Histología y Embriología, Facultad de Medicina, Universidad de la República. Av. Gral. Flores 2125. 11800, Montevideo, Uruguay
3) Laura Martínez-Palma: lmartinezpalma07@gmail.com
Departamento de Histología y Embriología, Facultad de Medicina, Universidad de la República. Av. Gral. Flores 2125. 11800, Montevideo, Uruguay
4) Adriana Cassina: adrianamariacassina@gmail.com
Departamento de Bioquímica, Centro de Investigaciones Biomédicas (CEINBIO), Facultad de Medicina, Universidad de la República. Av. Gral. Flores 2125. 11800, Montevideo, Uruguay
5) Patricia Cassina, pcassina@fmed.edu.uy / patricia.cassina@gmail.com
Departamento de Histología y Embriología, Facultad de Medicina, Universidad de la República. Av. Gral. Flores 2125. 11800, Montevideo, Uruguay

FUNDING: This work was supported by Grant # FCE_1_2019_1_156461 from the Agencia Nacional de Innovación e Investigación (ANII), Uruguay, to PC and Programa de Desarrollo de Ciencias Básicas (PEDECIBA, MEC-UdelaR to PC and EM.

ETHICS STATEMENT: Procedures using laboratory animals were in accordance with international guidelines and were approved by the Institutional Animal Committee: Comisión Honoraria de Experimentación Animal de la Universidad de la República (CHEA; https://chea.edu.uy/); protocol # 1038.

DATA AVAILABILITY: The data that support the findings of this study are available from the corresponding author upon reasonable request.

CONFLICT OF INTEREST: The authors declare no conflict of interest.

Pyruvate dehydrogenase kinase 2 knockdown restores the ability of ALS-linked SOD1G93A rat astrocytes to support motor neuron survival by increasing mitochondrial respiration

Running title: PDK knockdown and ALS astrocyte toxicity

Ernesto Miquel[1], Rosalía Villarino[1], Laura Martínez-Palma[1], Adriana Cassina [2], Patricia Cassina[1]

1) Departamento de Histología y Embriología, Facultad de Medicina, Universidad de la República. Av. Gral. Flores 2125. 11800, Montevideo, Uruguay
2) Departamento de Bioquímica, Centro de Investigaciones Biomédicas (CEINBIO), Facultad de Medicina, Universidad de la República. Av. Gral. Flores 2125. 11800, Montevideo, Uruguay

Acknowledgments:
This work was supported by Grant # FCE_1_2019_1_156461 from the Agencia Nacional de Innovación e Investigación (ANII), Uruguay, to PC and Programa de Desarrollo de las Ciencias Básicas (PEDECIBA, MEC-UdelaR to PC and EM. We thank Dr. Homero Rubbo (Facultad de Medicina, Universidad de la República, Uruguay) for critical comments on the manuscript.

Word count:
Total word count of the manuscript: 8159 words
Abstract: 249 words
Introduction: 603 words
Materials and Methods: 2239 words
Results: 1119 words
Discussion: 1376 words
Acknowledgments: 53 words
References: 1996 words
Figure Legends: 524 words

Abstract:

Amyotrophic lateral sclerosis (ALS) is characterized by progressive motor neuron (MN) degeneration. Various studies using cellular and animal models of ALS indicate that there is a complex interplay between MN and neighboring non-neuronal cells, such as astrocytes, resulting in non-cell autonomous neurodegeneration. Astrocytes in ALS exhibit a lower ability to support MN survival than non-disease-associated ones, which is strongly correlated with low mitochondrial respiratory activity. Indeed, pharmacological inhibition of pyruvate dehydrogenase kinase (PDK) led to an increase in the mitochondrial oxidative phosphorylation

pathway as the primary source of cell energy in SOD1G93A astrocytes and restored the survival of MN. Among the four PDK isoforms, PDK2 is ubiquitously expressed in astrocytes and presents low expression levels in neurons. Herein, we hypothesize whether selective knockdown of PDK2 in astrocytes may increase mitochondrial activity and, in turn, reduce SOD1G93A-associated toxicity. To assess this, cultured neonatal SOD1G93A rat astrocytes were incubated with specific PDK2 siRNA. This treatment resulted in a reduction of the enzyme expression with a concomitant decrease in the phosphorylation rate of the PDH complex. In addition, PDK2-silenced SOD1G93A astrocytes exhibited restored mitochondrial bioenergetics parameters, adopting a more complex mitochondrial network. This treatment also decreased lipid droplet content in SOD1G93A astrocytes, suggesting a switch in energetic metabolism. Significantly, PDK2 knockdown increased the ability of SOD1G93A astrocytes to support motor neuron survival, further supporting the major role of astrocyte mitochondrial respiratory activity in astrocyte-MN interactions. These results suggest that PDK2 silencing could be a cell-specific therapeutic tool to slow the progression of ALS.

Keywords: PDK2, astrocytes, mitochondria, ALS

Main Points:

Silencing PDK2 in SOD1G93A astrocytes reduces PDH phosphorylation.
Silenced astrocytes recover mitochondrial bioenergetics and morphology.
This metabolic reprogramming restores the ability of astrocytes to support motor neuron survival.

Introduction:

Amyotrophic lateral sclerosis (ALS) is a progressive neurodegenerative disease characterized by the gradual loss of motor neurons (MNs) in the spinal cord, brain stem, and motor cortex, which in turn induce voluntary muscle atrophy (Al-Chalabi et al., 2016). The cellular mechanisms determining neuronal death are still under research, and many have been proposed, including mitochondrial dysfunction (Smith, Shaw, & De Vos, 2019). In ALS patients and animal models of the disease, reactive astrocytes surround both upper and lower degenerating MNs, and evidence indicates that they play a crucial role in the pathology (Taylor, Brown, & Cleveland, 2016). Successive studies have shown that surrounding glial cells, particularly astrocytes, critically influence MN survival (Clement et al., 2003). Co-culture assays have clearly stated a reduced ability of astrocytes to support motor neuron survival in ALS models, whether the cells originate from embryonic stem cells (Di Giorgio, Carrasco, Siao, Maniatis, & Eggan, 2007), human IPSCs (Haidet-Phillips et al., 2011), mice (Nagai et al., 2007) or rat cells (Vargas, Pehar, Cassina, Beckman, & Barbeito, 2006). We have previously described that a metabolic switch characterized by reduced mitochondrial respiration underlies the astrocyte-mediated toxicity to MNs (Miquel et al., 2012). In primary astrocyte cultures obtained from the transgenic (Tg) ALS-linked mutated SOD1G93A rats (SOD1G93A astrocytes), treatment with the metabolic modulator dichloroacetate (DCA) enhanced both their

mitochondrial respiratory activity and ability to support motor neuron survival in co-culture. In addition, DCA administration to SOD1G93A mice reduced neuronal death and increased survival (Miquel et al., 2012). DCA is an inhibitor of the pyruvate dehydrogenase kinases (PDKs), which phosphorylate the E1α subunit of the pyruvate dehydrogenase (PDH) complex (PDC) and suppress the catalysis of pyruvate to acetyl-CoA (Holness, Bulmer, Smith, & Sugden, 2003). Inhibition of PDK keeps most of PDH in the active form, and therefore, pyruvate metabolism switches towards glucose oxidation to CO_2 in the mitochondria. The PDH/PDK system acts as a key regulator of mitochondrial respiration. It plays an essential role in the metabolic switch from oxidative phosphorylation (OXPHOS) to aerobic glycolysis that accompanies malignant transformation in cancer (W. Zhang, Zhang, Hu, & Tam, 2015).

PDC is a multisubunit protein that is composed of pyruvate dehydrogenase (E1), dihydrolipoyl acetyltransferase (E2), dihydrolipoyl dehydrogenase (E3), and E3-binding protein (E3BP) subunits that concertedly convert pyruvate to acetyl-CoA (Patel & Roche, 1990). All subunits are expressed in astrocytes and neurons, but astrocytes show significantly higher immunoreactivities for all of them than neurons (Halim et al., 2010).

Besides the differential expression of its constituent proteins, PDC activity is regulated by several mechanisms, such as allosteric inhibition by acetyl CoA and NADH. However, the main mechanism for maintaining long-term control over metabolic processes is through covalent modification of the enzyme. The reversible phosphorylation of PDH-E1α that regulates PDC activity (Patel & Korotchkina, 2006) is accomplished by four different PDKs (PDK1-4) and two different phosphatases (PDP1-2), which are all differentially expressed in mammalian tissues (Bowker-Kinley, Davis, Wu, Harris, & Popov, 1998). The regulation of PDC at the protein expression or activity levels contributes to the differential metabolic phenotype of neurons and astrocytes (Halim et al., 2010). **In addition,** there are different expression levels of PDH kinases and phosphatases between both cell types (Halim et al., 2010)**.** Indeed, control of PDK expression levels allows cells and tissues to regulate PDC activity and, therefore, glucose oxidation rates and mitochondrial respiration (Lydell et al., 2002). **While PDK1 and PDK3 are present in both cell types**, with slightly higher expression of PDK1 in neurons, PDK2 and PDK4 levels are significantly superior in astrocytes compared to neurons (Halim et al., 2010), which is consistent with the higher PDHα phosphorylation status, lower PDC activity and higher lactate production displayed by these cells (Pellerin & Magistretti, 2012). **These different profiles of PDK isoform expression between astrocytes and neurons offer a key target to regulate mitochondrial respiration specifically in astrocytes. In particular, the PDK2 isoform has been previously reported to be enhanced in astrocytes during diabetes, where it determines phosphorylated-PDH (p-PDH), causing a glycolytic metabolic shift along with substantial inflammation**(Rahman et al., 2020,) **which prompted us to select this isoform for this study.**

Here, we tested the hypothesis of whether silencing PDK2 may enhance mitochondrial respiratory function in SOD1G93A expressing astrocytes and, in turn, improve their capacity to support MN survival.

Materials and Methods

Materials

Culture media and serum were from Gibco (Thermo Fisher Scientific). Culture flasks and plates were from Nunc (Thermo Fisher Scientific). siRNAs were purchased from Ambion (Thermo Fisher Scientific). DCA and all other reagents were from Sigma-Aldrich (Merck) unless otherwise specified.

Ethics Statement

Procedures using laboratory animals were in accordance with international guidelines and were approved by the Institutional Animal Committee: Comisión Honoraria de Experimentación Animal de la Universidad de la República (CHEA; https://chea.edu.uy/); protocol # 1038.

Animals

Rats (*Rattus norvegicus*) were housed (up to 6 female or male animals per cage) in a centralized animal facility with a 12-h light-dark cycle with ad libitum access to food and water. Male hemizygous NTac:SD-Tg(SOD1G93A)L26H rats (RRID:IMSR_TAC:2148), obtained from Taconic (Hudson, NY), were bred locally with outbred Sprague–Dawley background. The progenies were genotyped by polymerase chain reaction (PCR), as previously described (Howland et al., 2002).

Primary Cell Cultures

Neonatal rat astrocyte cultures were prepared from Tg SOD1G93A or non-Tg 1-day-old pups (without regard to sex) genotyped by PCR, according to the procedures of Saneto and De Vellis (Saneto & De Vellis, 1987) with minor modifications (Cassina et al., 2002). Briefly, spinal cords were dissected, meninges were carefully removed, and tissue was chopped and dissociated with 0.25% trypsin-EDTA for 25 min at 37 °C. Trypsinization was stopped with high-glucose (4.5 g/l), pyruvate-free Dulbecco's modified Eagle's medium (DMEM) supplemented with HEPES (3.6 g/l), penicillin (100 IU/mL), streptomycin (100 mg/mL), and 10% (v/v) fetal bovine serum (FBS) (s-DMEM medium) in the presence of 50 µg/mL DNase I. After mechanical disaggregation by repeated pipetting, the suspension was passed through an 80-µm mesh and spun for 10 min at 300×g. The pellet was resuspended in s-DMEM medium and plated at a density of 1.5×10^6 cells per 25-cm^2 tissue culture flask. When confluent, cultures were shaken for 48 h at 250 rpm, incubated for another 48 h with 10 µM cytosine arabinoside, and then plated at a density of 2×10^4 cells/cm^2 in 4-well plates for co-cultures, Seahorse xFE24 plates for respirometry assays, or Lab-Tek 4-well chambered coverglass for mitochondrial or lipid droplets imaging studies.

Astrocyte-MN co-cultures: MN preparations were obtained from embryonic day 15 (E15) rat spinal cord by a combination of optiprep (1:10, SIGMA St. Louis, MO) gradient centrifugation and immunopanning with the monoclonal antibody IgG192 against p75 neurotrophin receptor as previously described (Cassina et al., 2002), then plated on rat astrocyte monolayers at a density of 300 cells/cm^2 and maintained for 48 h in Leibovitz's L-15 medium supplemented with 0.63 mg/mL bicarbonate, 5 µg/mL insulin, 0.1 mg/mL conalbumin, 0.1 mM putrescine, 30 nM sodium selenite, 20 nM progesterone, 20 mM glucose, 100 IU/mL penicillin, 100 µg/mL

streptomycin, and 2% horse serum (HS) (s-L15 medium) as described (Cassina et al., 2002). Astrocyte treatments were done 24 h prior to MN addition, and the astrocyte monolayers were washed twice with PBS to remove traces of the different treatments before plating the MNs.

siRNA transfection

80% confluent spinal cord astrocyte monolayers were changed to Dulbecco's modified Eagle's medium supplemented with 2% fetal bovine serum before treatment. siRNA transfection was performed using Lipofectamine 2000 (Invitrogen) according to the manufacturer's instructions. Astrocytes were transfected with 40 nM of Silencer Select pre-designed siRNAs (Ambion) targeting PDK2 mRNA, PDK1 mRNA, or negative control siRNA (NC siRNA no. 1) 24 h before either total RNA isolation using TRIzol reagent (Invitrogen) for quantitative PCR or 48h before lysis for western blot or before co-culture experiments. Three different siRNA for PDK2 were tested, and the sequence that achieved a more pronounced reduction of PDK2 expression was selected for the rest of the studies.

Western Blot

Astrocyte monolayers were treated with siRNA as described above, or 5 mM DCA. After 48 h of treatment, proteins were extracted from cells in 1% SDS supplemented with 2 mM sodium orthovanadate and Complete protease inhibitor cocktail (Roche). Lysates were resolved by electrophoresis on 12% SDS-polyacrylamide gels and transferred to a nitrocellulose membrane (Thermo). The membrane was blocked for 1 h at room temperature (RT) in 5% bovine serum albumin (BSA) in PBS-T (Phosphate-buffered saline with 0.1% Tween). The membrane was then probed overnight with primary antibodies in 5% BSA in PBS-T at 4 ºC, washed in PBS-T, and probed with the appropriate secondary antibodies for 60 min at RT. Primary antibodies were rabbit polyclonal phosphodetect anti- PDH-E1a(pSer293) (AP1062; Calbiochem; RRID:AB_10616069; 1:800), mouse anti Pyruvate Dehydrogenase E1-alpha subunit (Abcam Cat# ab110334, RRID:AB_10866116; 1:800), and mouse anti ß-actin (Sigma-Aldrich Cat# A5441, RRID:AB_476744; 1:4000) as loading control. The secondary antibodies used were IRDye® 800CW Goat anti-Mouse IgG antibody (LI-COR Biosciences Cat# 926-32210, RRID:AB_621842) and IRDye® 680RD Goat anti-Rabbit IgG antibody (LI-COR Biosciences Cat# 925-68071, RRID:AB_2721181). Detection and quantification were performed with a LI-COR Odyssey imaging system and included software. The relative levels of pSer293 E1a PDH and total E1a PDH were quantified. The pSer293 to total E1a ratio was calculated and normalized against vehicle-treated cells.

qPCR

Total astrocyte RNA was isolated using Trizol reagent (Thermo Fisher Scientific), followed by chloroform extraction and isopropanol precipitation. Possible DNA contaminations were eliminated with DNase treatment using DNase-free Kit (Thermo Fisher Scientific). RNA quality was evaluated by agarose gel electrophoresis followed by ethidium bromide staining and quantified using a NanoDrop 1000 Spectrophotometer (Thermo Fisher Scientific; RRID:SCR_016517). 500 ng of this total RNA was reverse-transcribed using 200 U M-MLV-reverse transcriptase (Thermo Fisher Scientific) following manufacturer instructions. 25 ng of the resulting cDNA was diluted in Biotools Quantimix Easy master mix (Biotools) in 10 µl

250 volume. All reactions were performed in triplicates in strip tubes (Axygen), using specific
251 forward and reverse primers. The sequences of the quantitative PCR primers (IDT, Integrated
252 DNA Technologies) used were as follows: for GAPDH F: 5'-CAC TGA GCA TCT CCC TCA CAA-3'
253 and R: 5'-TGG TAT TCG AGA GAA GGG AGG-3', for PDK2 F: 5'- TCA GCT AGG GGC CTT CTC TT-3'
254 and R: 5'- CCG TAC CCC AGG GGA TAG AT-3'. According to the sample, we used cycles 15–23
255 (the threshold cycle, Ct) to calculate the relative amounts of our gene of interest. PCR
256 amplification was done over 40 cycles using a Rotor-Gene 6000 System (Corbett Life Science),
257 and data were analyzed using Rotor-Gene 6000 software (Corbett Life Science;
258 RRID:SCR_017552). Quantification was performed with the ΔΔCt method using astrocytes
259 treated with vehicle as a negative control and GAPDH mRNA as reference.
260

261 ## Oxygen consumption rate assays

262 Oxygen consumption rate (OCR) and extracellular acidification rate (ECAR) were measured
263 simultaneously in a Seahorse XFe24 extracellular flux analyzer (Agilent; RRID:SCR_019539).
264 Before the experiment, the culture medium was replaced with an unbuffered medium (DMEM
265 pH 7.4, supplemented with 5 mM glucose, 1 mM sodium pyruvate, 32 mM NaCl, and 2 mM
266 glutamine) and incubated for 1 h at 37 °C without CO_2. Basal oxygen consumption
267 measurements were taken at the beginning of the assay, followed by the sequential addition
268 of oligomycin (0.5 µM), carbonyl cyanide 4-(trifluoromethoxy)phenylhydrazone (FCCP; 2 µM),
269 and antimycin A (AA; 1 µM) + rotenone (1 µM). The following bioenergetics parameters were
270 determined: Basal respiration: (last OCR measurement before oligomycin injection) -
271 (minimum OCR after rotenone/antimycin A addition); **proton leak**: (oligomycin-resistant
272 respiration) - (minimum OCR after rotenone/antimycin A addition); Respiration linked to ATP
273 production: (last OCR measurement before oligomycin injection) - (minimum OCR after
274 oligomycin addition); Maximal respiration: (maximum OCR after FCCP addition) - (minimum
275 OCR after rotenone/antimycin A addition); Spare respiratory capacity: Maximal respiration -
276 Basal respiration. After each assay, protein content (µg) per well was determined with the
277 bicinchoninic acid (BCA) technique. OCRs and ECARs were normalized considering protein
278 content (µg). Respiratory Indexes were determined as ratios between the respiratory rates
279 obtained in different conditions, which are therefore internally normalized and independent of
280 cell number or protein mass (Brand & Nicholls, 2011). These include Coupling efficiency (ratio
281 between respiration linked to ATP synthesis and basal respiration) and Respiratory Control
282 Ratio (RCR; the ratio between maximum and oligomycin-resistant respiration rates).
283

284 ## Fluorescent Labeling of Mitochondria

285 Confluent astrocyte monolayers seeded on 4-well Nunc™ Lab-Tek™ chambered coverglass
286 (Thermo Scientific) were treated as indicated above with vehicle, NC siRNA, PDK2 siRNA, or 5
287 mM DCA. After 48 h, the cells were incubated with 100 nM MitoTracker Green FM
288 (Thermo/Invitrogen, Cat# M7514) in Dulbecco's Modified Eagle Medium (DMEM) for 30 min in
289 a 37 ºC incubator at 5% CO2 and 95% humidity. Following incubation, cells were washed in
290 warm DMEM and visualized by confocal microscopy. Confocal image stacks were acquired with
291 a Leica TCS-SP5-II confocal microscope (Leica Microsystems) using an HCX PL APO 63x/1.40 oil
292 immersion objective, with 0.2 µm z-stack slice intervals and at least 10 slices per cell. Images
293 were obtained for at least 25 cells per group from 4 independent experiments.
294

295 ## Mitochondrial morphology analysis
296 Confocal image stacks were deconvolved with Huygens Professional version 19.10 (Scientific
297 Volume Imaging, The Netherlands). Mitochondrial morphology was analyzed using Fiji (ImageJ)
298 software (NIH; RRID:SCR_002285) as follows: Image stacks corresponding to individual cells
299 were extracted from each confocal stack. Images were converted to binary by thresholding
300 and processed to remove noise and outlier voxels. Mitochondrial skeleton profiles were
301 obtained with the built-in Skeletonize feature, and morphology was analyzed with the skeleton
302 analysis plugin, which measures the length of each branch and the number of branches in each
303 skeletonized feature, from which parameters describing mitochondrial network morphology
304 were calculated. Distinct mitochondrial morphologies were identified and classified as
305 individuals (puncta and rods) or networks as previously reported (Leonard et al., 2015;
306 Valente, Maddalena, Robb, Moradi, & Stuart, 2017): punctate mitochondria are defined as
307 small point-like structures, whereas rods are elongated without being branched. Networks are
308 characterized by connected branches. In the skeleton analysis, individuals (puncta or rods)
309 have no junctions, while networks are structures with at least one junction. We quantified the
310 number of 'individual' structures with no branches (puncta and rods), the number of networks,
311 mean mitochondrial length, and mean length of rods/network branches (mean rod/branch
312 length). For this last parameter, we considered rods and network branches together (puncta
313 are not included), as the biological forces increasing rod length and those increasing the length
314 of network branches should essentially be the same (Valente et al., 2017). Data from at least
315 25 cells per treatment were analyzed and repeated in four independent experiments.
316
317 ## Lipid droplets labeling and quantification
318 Subconfluent astrocyte monolayers seeded on 4-well Nunc™ Lab-Tek™ chamber slides
319 (Thermo Scientific) were treated as indicated above with vehicle, NC siRNA, PDK2 siRNA, or 5
320 mM DCA in DMEM with 2% Foetal Bovine Serum. 48 h later, cells were washed with PBS, fixed
321 with 4% paraformaldehyde in PBS for 18 min on ice, and washed twice with PBS. Then, cells
322 were permeabilized with 0.2% Triton X-100 in PBS for 30 min followed by incubation with
323 blocking solution (BS): 10 % goat serum, 2% bovine serum albumin, 0,1% triton X-100 in PBS
324 for 1 h at RT. Cells were incubated overnight with rabbit anti glial fibrillary acidic protein
325 (GFAP) antibody (1:500; Sigma-Aldrich #G9269, RRID:AB_477035) in BS at RT, followed by
326 washing three times in PBS and incubation with Alexa Fluor 488-conjugated goat anti-rabbit
327 IgG secondary antibody (1:1000, Thermo Fisher Scientific, # A-11034, RRID:AB_2576217) for 1
328 h at RT. After washing twice with PBS, cells were incubated for 30 min at RT with Oil Red O
329 (ORO) working solution (ORO stock solution: 0.625% ORO in 99% (vol/vol) isopropyl alcohol
330 prepared by stirring for 2 h at RT; ORO working solution: 1.5 parts of ORO stock solution to one
331 part of distilled water, incubated for 10 min at 4 °C, and filtered through a 45-µm filter to
332 remove precipitates). Following incubation, cells were washed thrice with deionized water,
333 incubated with Hoechst 33342 (1 µg/mL; Sigma-Aldrich #14533) for 15 min at RT to label
334 nuclei, and mounted in 80% glycerol in PBS. Cell images were acquired using a Nikon Eclipse
335 E400 epifluorescence microscope (Nikon) coupled with a Nikon Ds-Fi3 camera, using a 40x
336 objective. At least 25 images were obtained per group from 3 independent experiments.
337 Lipid Droplet (LD) quantification: LD images were binarized by thresholding using Fiji (ImageJ)
338 software (NIH; RRID:SCR_002285), **followed by watershed processing to resolve overlapping**
339 **structures.** Particles in each image were counted and analyzed using the "Analyze particles"

340 command. The number of LD per cell was estimated as the ratio of LD to the number of nuclei
341 in each image.
342

343 MN survival assay

344 Co-cultures were fixed (4% paraformaldehyde plus 0.1% glutaraldehyde in PBS, 15 min on ice)
345 and washed twice with PBS. Then, cells were permeabilized with 0.2% Triton X-100 in PBS for
346 30 min followed by incubation with BS: 10 % goat serum, 2% bovine serum albumin, 0,1%
347 triton X-100 in PBS for 1 h at RT. Cells were incubated overnight with rabbit anti-beta-III
348 tubulin antibody (1:3000; Abcam, #ab18207 RRID: AB_444319) in BS at 4 ºC. After washing
349 three times with PBS, cells were incubated with horseradish peroxidase-conjugated goat anti-
350 rabbit IgG secondary antibody (1:500, Thermo Fisher Scientific, #31,460, RRID: AB_228341) for
351 1 h at RT, followed by three washes with PBS and 3,3'-diaminobenzidine developing. MN
352 survival was evaluated by direct counting of cells displaying neurites longer than four cell
353 bodies diameter (Cassina et al., 2002; Martínez-Palma et al., 2019) using a Nikon Eclipse TE 200
354 microscope.
355

356 Statistics

357 All data analysis and statistics were performed using GraphPad Prism 9 software
358 (RRID:SCR_002798). Data are presented as mean ± SEM of values obtained from at least three
359 independently prepared cultures performed in duplicates or triplicates. Tests used were
360 ordinary one-way ANOVA followed by Tukey's post hoc multiple comparisons. Statistical
361 signification was determined at $p < 0.05$.

362 Results

363 1) Silencing PDK2 mRNA reduced phosphorylated PDH in cultured
364 astrocytes

365 To down-regulate PDK2 expression in cultured astrocytes, confluent astrocyte monolayers
366 were incubated with siRNA for PDK2, PDK1, or negative control (NC) siRNA without targets,
367 then PDK2 mRNA expression was detected by qPCR. A reduction in PDK2 mRNA expression
368 was successfully achieved only when siRNA against PDK2 was employed (Figure 1A). Neither
369 PDK1 siRNA nor the negative control (NC) demonstrated any downregulation of PDK2 mRNA
370 expression.

371 Notably, PDK activity, assessed as the ratio of phosphorylated to total PDH measured by
372 immunoblotting against specific antibodies, was significantly decreased in PDK2 siRNA-treated
373 astrocytes with no variation in total PDH immunoreactivity (Figure 1B). No
374 phosphorylated/total PDH ratio difference was found in PDK1 siRNA or NC siRNA-treated
375 astrocytes.

376 **Furthermore, PDK2 siRNA specifically targeted the PDK2 isoform and did not affect PDK4**
377 **mRNA expression, which is the other isoform highly expressed in astrocytes** (Guttenplan et
378 al., 2020; Halim et al., 2010; Hasel, Rose, Sadick, Kim, & Liddelow, 2021; Y. Zhang et al., 2014)
379 **(Figure 1C).**

380

2) PDK2 mRNA knockdown in SOD1G93A expressing astrocytes increases mitochondrial bioenergetic parameters.

To study whether PDK2 knockdown could increase the mitochondrial respiration of SOD1G93A astrocytes, confluent SOD1G93A astrocytes were incubated with siRNA for PDK2 or NC siRNA, and OCR was measured before and after the addition of specific inhibitors and an uncoupler of the respiratory chain and OXPHOS as indicated in methods. As previously reported (Miquel et al., 2012), reduced respiratory capacity was detected in SOD1G93A astrocytes compared to non-Tg astrocytes. Silencing PDK2 mRNA or DCA exposure enhanced OCR in SOD1G93A astrocytes to the extent found in the non-Tg ones (Figure 2A).

SOD1G93A astrocytes exhibited reduced basal, ATP production-linked, and maximal respiration compared to non-Tg astrocytes (Figure 2B), as previously reported for other SOD1G93A-expressing cell types (Pharaoh et al., 2019). Upon PDK2 siRNA or DCA treatment, ATP production-linked and maximal respiration were significantly increased in SOD1G93A astrocytes (Figure 2B). No significant change in basal respiration was observed following PDK2-siRNA or DCA treatment. No changes were seen in non-mitochondrial or **proton leak respiration** in any treatment group.
In addition, spare respiratory capacity and the respiratory indexes coupling efficiency and respiratory control ratio (RCR) were reduced in SOD1G93A-expressing compared to non-Tg astrocytes (Figure 2C). This indicates a reduced ability of the electron transport chain to respond to an increase in energy demand, a lower coupling of the electron transport chain to ADP phosphorylation, and a diminished overall mitochondrial respiratory function, respectively (Brand & Nicholls, 2011). PDK2 knockdown or DCA treatment showed a significant increase in all these indexes to the level shown by non-Tg astrocytes.

3) PDK2 mRNA knockdown in SOD1G93A astrocytes modifies mitochondrial network morphology.

The improvement of mitochondrial respiratory function in PDK2-silenced SOD1G93A astrocytes was associated with morphological changes in the mitochondrial network as detected by live confocal microscopy with mitotracker green labeling (Figure 3). After imaging processing involving binarization and skeleton analysis, two types of mitochondrial structures were recognized: networks (mitochondrial structures with at least three branches) and individuals (isolated mitochondria, which could be punctate -a single pixel in the skeletonized image- or rods -unbranched structures with two or more pixels in the skeletonized image-), as previously reported (Bakare et al., 2021; Valente et al., 2017). Smaller individual mitochondria and more fragmented networks were found in SOD1G93A astrocytes compared to the filamentous mitochondrial network morphology exhibited by non-Tg astrocytes (Figure 3A). This is in agreement with previous reports on SOD1G93A-expressing glial cells (Jiménez-Riani et al., 2017; Joshi et al., 2019; Martínez-Palma et al., 2019). In contrast, when treated with DCA or PDK2 siRNA, SOD1G93A astrocytes exhibit a mitochondrial network morphology reminiscent of that of non-Tg astrocytes (Figure 3A). Consequently, mean mitochondrial length (including all branches), as well as mean mitochondrial rod/branch length (mean length of rod-like mitochondria or branches in mitochondrial networks), was significantly reduced in

423 SOD1G93A astrocytes compared to non-Tg ones (Figure 3B). These parameters were increased
424 in PDK2 siRNA or DCA-treated SOD1G93A astrocytes to the level of non-Tg astrocytes but were
425 not in NC siRNA-treated SOD1G93A astrocytes (Figure 3B). In addition, the percentage of
426 mitochondria adopting a network-like interconnected morphology was reduced in SOD1G93A
427 astrocytes (where there was a higher percentage of isolated mitochondria) compared to non-
428 Tg astrocytes, and it was significantly increased in the case of cells treated with PDK2 siRNA or
429 DCA, to a similar level as in non-Tg astrocytes.
430

431 4) PDK2 Knockdown reduced lipid droplets accumulation in SOD1G93A 432 astrocytes

433 Inhibition of mitochondrial respiration is associated with lipid droplet accumulation in various
434 cell types, including glial cells (Liu et al., 2015). In addition, SOD1G93A-expressing glial cells
435 exhibit increased lipid inclusions (Jiménez-Riani et al., 2017). Therefore, we analyzed whether
436 PDK silencing may affect these organelles in SOD1G93A astrocytes. Examination of Oil red O-
437 stained astrocytes showed cytoplasmic accumulation of labeled round bodies of varying size
438 surrounding the cell nucleus, an image consistent with lipid droplets (LD; Figure 4A). LD
439 exhibited a heterogeneous distribution across the astrocyte monolayer. Quantification of the
440 number of LDs per cell revealed the previously reported increase in the number of LDs in
441 SOD1G93A astrocytes (Velebit et al., 2020) relative to non-Tg astrocytes. Importantly, there
442 was a significant reduction in LD following silencing or pharmacological inhibition of PDK2 in
443 SOD1G93A astrocytes (Figure 4B).

444

445 5) PDK2 knockdown enhanced the ability of SOD1G93A astrocytes to 446 support motor neuron survival

447 Next, the effect of PDK2 silencing on SOD1G93A astrocyte toxicity to motor neurons (MNs)
448 was assessed. As previously reported (Vargas et al., 2006), SOD1G93A astrocytes exhibited a
449 reduced ability to support MN survival compared to non-Tg ones. The number of MNs that
450 survived after 72 h on top of SOD1G93A astrocyte monolayers was reduced by ~50% compared
451 to that obtained from non-Tg astrocyte/MN co-cultures. Silencing PDK2 mRNA on SOD1G93A-
452 expressing astrocytes significantly increased MN survival in co-culture to the level reached on
453 top of non-Tg astrocytes or DCA-treated SOD1G93A astrocytes. In addition, incubation of
454 SOD1G93A with NC siRNA had no effect on MN survival (Figure 5A).

455

456 Discussion

457 Herein, we demonstrate that downregulation of the major astrocytic PDK isoform (PDK2)
458 expression in SOD1G93A-bearing astrocytes modulates the energy phenotype profile, inducing
459 a metabolic switch characterized by an increase in mitochondrial respiratory function and a
460 remodeling of the mitochondrial network morphology to the level of non-Tg astrocytes.
461 Importantly, this selective mRNA knockdown improves the ability of SOD1G93A astrocytes to
462 support motor neuron survival. Our results further strengthen the hypothesis that
463 mitochondrial function in astrocytes is crucial to sustaining motor neuron survival in ALS.

Cell-to-cell communication critically influences MN survival in ALS. We and others have reported that SOD1G93A astrocytes and aberrant glial cells selectively kill surrounding MN (Di Giorgio et al., 2007; Díaz-Amarilla et al., 2011; Nagai et al., 2007; Vargas et al., 2006). We have proposed that a metabolic reprogramming characterized by reduced mitochondrial respiratory activity with a decreased capacity to respond to energetic demands occurs in SOD1G93A expressing astrocytes, which is critically associated with the reduced ability to maintain MN survival (Cassina, Miquel, Martínez-Palma, & Cassina, 2021). This was supported by the results of treating SOD1G93A astrocytes with the metabolic modulator DCA (Miquel et al., 2012). DCA-treated astrocytes presented increased mitochondrial bioenergetics and improved MN survival in co-culture. On top of that, oral administration of DCA to SOD1G93A animals increased survival associated with higher mitochondrial respiratory activity in the spinal cord and delayed MN survival, suggesting that metabolic modulation may offer a new therapeutic target to delay disease progression.

A key target in metabolic modulation is the PDC, a mitochondrial gatekeeping enzyme that links glycolysis with the citric acid cycle and the subsequent OXPHOS (Patel & Roche, 1990; Takubo et al., 2013). PDC is a large complex containing three core enzymatically active subunits: pyruvate dehydrogenase (PDH), dihydrolipoamide acetyltransferase, and dihydrolipoyl dehydrogenase (Hiromasa, Fujisawa, Aso, & Roche, 2004; Hitosugi et al., 2011). PDH directly oxidizes pyruvate (Fan et al., 2014) and harbors regulatory serine residues that act as phosphorylation targets (Kolobova, Tuganova, Boulatnivov, & Popov, 2001). The PDC is under tight and complex regulation by PDK isoforms 1–4, with expression in peripheral and central tissues (Jha et al., 2012). The previously mentioned role of DCA as a metabolic modulator is based on its known action as a PDK inhibitor, with positive effects on ALS models (Martínez-Palma et al., 2019; Miquel et al., 2012; Palamiuc et al., 2015). A more recently described PDK inhibitor, phenylbutyrate, has also shown promising effects in ALS (Del Signore et al., 2009; Paganoni et al., 2020; Ryu et al., 2005), even exhibiting a synergistic effect with DCA (Ferriero, Iannuzzi, Manco, & Brunetti-Pierri, 2015). The PDK2 isoform is one of the most abundant in astrocytes (Halim et al., 2010) and exhibits negligible expression levels in neurons. PDK2 isoform knockdown resulted in reduced PDK2 expression in cultured astrocytes and, more importantly, diminished PDH phosphorylation, leading to increased OXPHOS activity. Indeed, bioenergetic mitochondrial parameters and indexes were significantly increased by PDK2 knockdown or DCA treatment in SOD1G93A astrocytes. These results indicate that SOD1G93A astrocytes either have fewer mitochondria or their mitochondria undergo reduced respiratory activity, showing decreased ability to respond to energy demands. Significantly, this was reverted by the specific PDK2 siRNA treatment. These results indicate that the PDK2 isoform is a major determinant of astrocytic PDH activity state, as previously shown (Rahman et al., 2020).

Besides increasing mitochondrial respiratory function, the knockdown of PDK2 mRNA expression in SOD1G93A-bearing astrocytes modified their mitochondrial network morphology. During glial reactivity in ALS, astrocytes undergo a metabolic shift from OXPHOS to glycolysis, associated with mitochondrial morphology changes to adapt to the new metabolic system (Cassina et al., 2021). Mitochondria switches from a branched connected respiratory active elongated network into clustered, fragmented organelles with decreased OXPHOS, which has been previously described in several cell types (Galloway, Lee, & Yoon,

2012; Sauvanet, Duvezin-Caubet, di Rago, & Rojo, 2010) including SOD1G93A aberrant glial cells (Martínez-Palma et al., 2019). The significant decrease in mean mitochondrial length and the mean mitochondrial rod/branched length displayed by SOD1G93A astrocytes compared to non-Tg ones, along with fewer mitochondrial networks, indicate a higher organelle fragmentation in SOD1G93A astrocytes. PDK-silencing or DCA treatment induced a significant increase in the mentioned parameters, suggesting that mitochondria have coalesced into a complex network structure when increasing OXPHOS. Taken together, the detailed morphologic description and the respirometry data provide a complete overview of astrocyte mitochondria that may assist in identifying the subtle differences between healthy control and disease-associated SOD1G93A astrocytes.

The metabolic switch induced by PDK2 silencing reduced lipid droplets (LDs) content in SOD1G93A astrocytes. LDs are dynamic organelles that are regulated in response to different cellular and physiological conditions, including mitochondrial dysfunction (Renne & Hariri, 2021). The mitochondrial respiratory activity provides ATP and NADPH to support the synthesis of fatty acids and glycolytic precursors from the tricarboxylic acid cycle (e.g., citrate) for esterification into triacylglycerides in the endoplasmic reticulum and for the storage in LDs (Smolič, Zorec, & Vardjan, 2021). LDs increase in astrocytes submitted to hypoxia (Smolič, Tavčar, et al., 2021) or ROS toxicity (Islam et al., 2019). Interestingly, SOD1G93A astrocytes have been shown to increase ROS formation (Vargas et al., 2006), and SOD1G93A aberrant glial cells exhibit a high amount of LDs by TEM (Jiménez-Riani et al., 2017). Lipidomic analysis in the spinal cords of SOD1G93A rats showed an accumulation of lipids, mainly cholesteryl esters and ceramides, with further alterations linked to disease progression and a reduction in cardiolipin levels, reflecting mitochondrial adaptations (Chaves-Filho et al., 2019). The sequestration of lipids in droplets could reflect a protective mechanism against oxidative stress and lipotoxicity, avoiding lipid membrane peroxidation (Bailey et al., 2015; Olzmann & Carvalho, 2019). Our observation of LD reduction associated with an increase in mitochondrial OXPHOS activity further supports that a metabolic switch is occurring in SOD1G93A astrocytes after treatment.

A major finding of our work is that silencing PDK2 in SOD1G93A astrocytes restored their ability to support motor neuron survival **to the same extent achieved previously with mitochondrial-targeted strategies such as DCA or MitoQ** (Cassina et al., 2021)**. The exact mechanism by which PDK2 inhibition is protecting MN survival needs further research. The link between mitochondrial OXPHOS and astrocyte-dependent trophic activity to MNs has been previously demonstrated with DCA** (Martínez-Palma et al., 2019; Miquel et al., 2012)**, antioxidants and Nitric Oxide synthase inhibitors** (Cassina et al., 2008)**. As mitochondrial OXPHOS activity is a main source of RONS production, RONS-mediated signaling pathways may be involved in the trophic activity of astrocytes. In this sense, the antioxidant response mediated by the nuclear factor erythroid 2–related factor 2 (Nrf2) has been shown to maintain the capacity of astrocytes to support motor neuron survival** (Díaz-Amarilla et al., 2016; Vargas et al., 2006)**. Taken together, these studies suggest that "mitochondrial dysfunction" in SOD1G93A astrocytes is not due to** irreversible damage **to the organelles** but **rather** a metabolic adaptation to the neurodegenerative microenvironment. DCA is a PDK inhibitor (Stacpoole, 2017) with the same inhibitory action between different enzyme isoforms. **Higher expression of PDK2 and PDK4 is revealed in astrocytes compared to neurons**

(Halim et al., 2010)**,** which is consistent with the higher PDHα phosphorylation status, lower PDC activity, and higher lactate production displayed by cultured astrocytes (Pellerin & Magistretti, 2012). Then, PDK2 arises as a key target to modulate astrocytic mitochondrial function, reducing surrounding MN loss and inducing a disease-modifying effect in ALS.

Previous transcriptomic analysis of glial and neuron from mice expressing EGFP under the control of cell-specific regulatory genes reported higher expression of PDK4 mRNA in astrocytes compared to neurons (Y. Zhang et al., 2014, 2016)**. However, in astrocytes, higher expression levels of PDK2 compared to PDK4 have been reported in ALS mice** (Guttenplan et al., 2020)**. In addition, the fact that PDK2 siRNA had no effect on PDK4 mRNA expression in astrocytes provides additional support for the choice of PDK2 as a target for regulating metabolic status in astrocytes.**

Our results emphasize that mitochondrial function in astrocytes is a critical feature in maintaining the survival of neighboring MNs and indicate that inducing a cell-specific metabolic switch may offer a new therapeutic window to modulate astrocyte-mediated toxicity in ALS.

References

Al-Chalabi, A., Hardiman, O., Kiernan, M. C., Chiò, A., Rix-Brooks, B., & van den Berg, L. H. (2016). Amyotrophic lateral sclerosis: moving towards a new classification system. *The Lancet Neurology*, Vol. 15, pp. 1182–1194. https://doi.org/10.1016/S1474-4422(16)30199-5

Bailey, A. P., Koster, G., Guillermier, C., Hirst, E. M. A., MacRae, J. I., Lechene, C. P., … Gould, A. P. (2015). Antioxidant Role for Lipid Droplets in a Stem Cell Niche of Drosophila. *Cell*, *163*(2), 340–353. https://doi.org/10.1016/j.cell.2015.09.020

Bakare, A. B., Meshrkey, F., Lowe, B., Molder, C., Rao, R. R., Zhan, J., & Iyer, S. (2021). MitoCellPhe reveals mitochondrial morphologies in single fibroblasts and clustered stem cells. *American Journal of Physiology - Cell Physiology*, *321*(4), C735–C748. https://doi.org/10.1152/ajpcell.00231.2021

Bowker-Kinley, M. M., Davis, W. I., Wu, P., Harris, R. A., & Popov, K. M. (1998). Evidence for existence of tissue-specific regulation of the mammalian pyruvate dehydrogenase complex. *Biochemical Journal*, *329*(1), 191–196. https://doi.org/10.1042/bj3290191

Brand, M. D., & Nicholls, D. G. (2011). Assessing mitochondrial dysfunction in cells. *Biochemical Journal*, *435*(2), 297–312. https://doi.org/10.1042/BJ20110162

Cassina, P., Cassina, A., Pehar, M., Castellanos, R., Gandelman, M., de Leon, A., … Radi, R. (2008). Mitochondrial Dysfunction in SOD1G93A-Bearing Astrocytes Promotes Motor Neuron Degeneration: Prevention by Mitochondrial-Targeted Antioxidants. *Journal of Neuroscience*, *28*(16), 4115–4122. https://doi.org/10.1523/JNEUROSCI.5308-07.2008

589 Cassina, P., Miquel, E., Martínez-Palma, L., & Cassina, A. (2021). Glial Metabolic
590 Reprogramming in Amyotrophic Lateral Sclerosis. *Neuroimmunomodulation*, *28*(4), 204–
591 212. https://doi.org/10.1159/000516926

592 Cassina, P., Peluffo, H., Pehar, M., Martínez-Palma, L., Ressia, A., Beckman, J. S., … Barbeito, L.
593 (2002). Peroxynitrite triggers a phenotypic transformation in spinal cord astrocytes that
594 induces motor neuron apoptosis. *Journal of Neuroscience Research*, *67*(1), 21–29.
595 https://doi.org/10.1002/jnr.10107

596 Chaves-Filho, A. B., Pinto, I. F. D., Dantas, L. S., Xavier, A. M., Inague, A., Faria, R. L., …
597 Miyamoto, S. (2019). Alterations in lipid metabolism of spinal cord linked to amyotrophic
598 lateral sclerosis. *Scientific Reports*, *9*(1), 11642. https://doi.org/10.1038/s41598-019-
599 48059-7

600 Clement, A. M., Nguyen, M. D., Roberts, E. A., Garcia, M. L., Boillée, S., Rule, M., … Cleveland,
601 D. W. (2003). Wild-Type Nonneuronal Cells Extend Survival of SOD1 Mutant Motor
602 Neurons in ALS Mice. *Science*, *302*(5642), 113–117.
603 https://doi.org/10.1126/science.1086071

604 Del Signore, S. J., Amante, D. J., Kim, J., Stack, E. C., Goodrich, S., Cormier, K., … Ferrante, R. J.
605 (2009). Combined riluzole and sodium phenylbutyrate therapy in transgenic amyotrophic
606 lateral sclerosis mice. *Amyotrophic Lateral Sclerosis*, *10*(2), 85–94.
607 https://doi.org/10.1080/17482960802226148

608 Di Giorgio, F. P., Carrasco, M. A., Siao, M. C., Maniatis, T., & Eggan, K. (2007). Non–cell
609 autonomous effect of glia on motor neurons in an embryonic stem cell–based ALS model.
610 *Nature Neuroscience*, *10*(5), 608–614. https://doi.org/10.1038/nn1885

611 Díaz-Amarilla, P., Miquel, E., Trostchansky, A., Trias, E., Ferreira, A. M., Freeman, B. A., …
612 Rubbo, H. (2016). Electrophilic nitro-fatty acids prevent astrocyte-mediated toxicity to
613 motor neurons in a cell model of familial amyotrophic lateral sclerosis via nuclear factor
614 erythroid 2-related factor activation. *Free Radical Biology and Medicine*, *95*, 112–120.
615 https://doi.org/10.1016/j.freeradbiomed.2016.03.013

616 Díaz-Amarilla, P., Olivera-Bravo, S., Trias, E., Cragnolini, A., Martínez-Palma, L., Cassina, P., …
617 Barbeito, L. (2011). Phenotypically aberrant astrocytes that promote motoneuron
618 damage in a model of inherited amyotrophic lateral sclerosis. *Proceedings of the National*
619 *Academy of Sciences*, *108*(44), 18126–18131. https://doi.org/10.1073/pnas.1110689108

620 Fan, J., Kang, H.-B., Shan, C., Elf, S., Lin, R., Xie, J., … Chen, J. (2014). Tyr-301 Phosphorylation
621 Inhibits Pyruvate Dehydrogenase by Blocking Substrate Binding and Promotes the
622 Warburg Effect. *Journal of Biological Chemistry*, *289*(38), 26533–26541.
623 https://doi.org/10.1074/jbc.M114.593970

624 Ferriero, R., Iannuzzi, C., Manco, G., & Brunetti-Pierri, N. (2015). Differential inhibition of PDKs
625 by phenylbutyrate and enhancement of pyruvate dehydrogenase complex activity by
626 combination with dichloroacetate. *Journal of Inherited Metabolic Disease*, *38*(5), 895–
627 904. https://doi.org/10.1007/s10545-014-9808-2

628 Galloway, C. A., Lee, H., & Yoon, Y. (2012). Mitochondrial morphology—emerging role in
629 bioenergetics. *Free Radical Biology and Medicine*, *53*(12), 2218–2228.
630 https://doi.org/10.1016/j.freeradbiomed.2012.09.035

631 Guttenplan, K. A., Weigel, M. K., Adler, D. I., Couthouis, J., Liddelow, S. A., Gitler, A. D., &
632 Barres, B. A. (2020). Knockout of reactive astrocyte activating factors slows disease
633 progression in an ALS mouse model. *Nature Communications*, *11*(1), 1–9.
634 https://doi.org/10.1038/s41467-020-17514-9

635 Haidet-Phillips, A. M., Hester, M. E., Miranda, C. J., Meyer, K., Braun, L., Frakes, A., … Kaspar, B.
636 K. (2011). Astrocytes from familial and sporadic ALS patients are toxic to motor neurons.
637 *Nature Biotechnology*, *29*(9), 824–828. https://doi.org/10.1038/nbt.1957

638 Halim, N. D., Mcfate, T., Mohyeldin, A., Okagaki, P., Korotchkina, L. G., Patel, M. S., … Verma, A.
639 (2010). Phosphorylation status of pyruvate dehydrogenase distinguishes metabolic
640 phenotypes of cultured rat brain astrocytes and neurons. *Glia*, *58*(10), 1168–1176.
641 https://doi.org/10.1002/glia.20996

642 Hasel, P., Rose, I. V. L., Sadick, J. S., Kim, R. D., & Liddelow, S. A. (2021). Neuroinflammatory
643 astrocyte subtypes in the mouse brain. *Nature Neuroscience 2021 24:10*, *24*(10), 1475–
644 1487. https://doi.org/10.1038/s41593-021-00905-6

645 Hiromasa, Y., Fujisawa, T., Aso, Y., & Roche, T. E. (2004). Organization of the Cores of the
646 Mammalian Pyruvate Dehydrogenase Complex Formed by E2 and E2 Plus the E3-binding
647 Protein and Their Capacities to Bind the E1 and E3 Components. *Journal of Biological*
648 *Chemistry*, *279*(8), 6921–6933. https://doi.org/10.1074/jbc.M308172200

649 Hitosugi, T., Fan, J., Chung, T.-W., Lythgoe, K., Wang, X., Xie, J., … Chen, J. (2011). Tyrosine
650 Phosphorylation of Mitochondrial Pyruvate Dehydrogenase Kinase 1 Is Important for
651 Cancer Metabolism. *Molecular Cell*, *44*(6), 864–877.
652 https://doi.org/10.1016/j.molcel.2011.10.015

653 Holness, M. J., Bulmer, K., Smith, N. D., & Sugden, M. C. (2003). Investigation of potential
654 mechanisms regulating protein expression of hepatic pyruvate dehydrogenase kinase
655 isoforms 2 and 4 by fatty acids and thyroid hormone. *Biochemical Journal*, *369*(3), 687–
656 695. https://doi.org/10.1042/bj20021509

657 Howland, D. S., Liu, J., She, Y., Goad, B., Maragakis, N. J., Kim, B., … Rothstein, J. D. (2002).
658 Focal loss of the glutamate transporter EAAT2 in a transgenic rat model of SOD1 mutant-
659 mediated amyotrophic lateral sclerosis (ALS). *Proceedings of the National Academy of*
660 *Sciences*, *99*(3), 1604–1609. https://doi.org/10.1073/pnas.032539299

661 Islam, A., Kagawa, Y., Miyazaki, H., Shil, S. K., Umaru, B. A., Yasumoto, Y., … Owada, Y. (2019).
662 FABP7 Protects Astrocytes Against ROS Toxicity via Lipid Droplet Formation. *Molecular*
663 *Neurobiology*, *56*(8), 5763–5779. https://doi.org/10.1007/s12035-019-1489-2

664 Jiménez-Riani, M., Díaz-Amarilla, P., Isasi, E., Casanova, G., Barbeito, L., & Olivera-Bravo, S.
665 (2017). Ultrastructural features of aberrant glial cells isolated from the spinal cord of

666 paralytic rats expressing the amyotrophic lateral sclerosis-linked SOD1G93A mutation.
667 *Cell and Tissue Research*, *370*(3), 391–401. https://doi.org/10.1007/s00441-017-2681-1

668 Joshi, A. U., Minhas, P. S., Liddelow, S. A., Haileselassie, B., Andreasson, K. I., Dorn, G. W., &
669 Mochly-Rosen, D. (2019). Fragmented mitochondria released from microglia trigger A1
670 astrocytic response and propagate inflammatory neurodegeneration. *Nature*
671 *Neuroscience*, *22*(10), 1635–1648. https://doi.org/10.1038/s41593-019-0486-0

672 Kolobova, E., Tuganova, A., Boulatnivov, I., & Popov, K. M. (2001). Regulation of pyruvate
673 dehydrogenase activity through phosphorylation at multiple sites. *Biochemical Journal*,
674 *358*(1), 69. https://doi.org/10.1042/0264-6021:3580069

675 Leonard, A. P., Cameron, R. B., Speiser, J. L., Wolf, B. J., Peterson, Y. K., Schnellmann, R. G., …
676 Rohrer, B. (2015). Quantitative analysis of mitochondrial morphology and membrane
677 potential in living cells using high-content imaging, machine learning, and morphological
678 binning. *Biochimica et Biophysica Acta (BBA) - Molecular Cell Research*, *1853*(2), 348–360.
679 https://doi.org/10.1016/j.bbamcr.2014.11.002

680 Liu, L., Zhang, K., Sandoval, H., Yamamoto, S., Jaiswal, M., Sanz, E., … Bellen, H. J. (2015). Glial
681 Lipid Droplets and ROS Induced by Mitochondrial Defects Promote Neurodegeneration.
682 *Cell*, *160*(1–2), 177–190. https://doi.org/10.1016/j.cell.2014.12.019

683 Lydell, C. P., Chan, A., Wambolt, R. B., Sambandam, N., Parsons, H., Bondy, G. P., … Allard, M. F.
684 (2002). Pyruvate dehydrogenase and the regulation of glucose oxidation in hypertrophied
685 rat hearts. *Cardiovascular Research*, *53*(4), 841–851. https://doi.org/10.1016/s0008-
686 6363(01)00560-0

687 Martínez-Palma, L., Miquel, E., Lagos-Rodríguez, V., Barbeito, L., Cassina, A., & Cassina, P.
688 (2019). Mitochondrial Modulation by Dichloroacetate Reduces Toxicity of Aberrant Glial
689 Cells and Gliosis in the SOD1G93A Rat Model of Amyotrophic Lateral Sclerosis.
690 *Neurotherapeutics*, *16*(1), 203–215. https://doi.org/10.1007/s13311-018-0659-7

691 Miquel, E., Cassina, A., Martínez-Palma, L., Bolatto, C., Trías, E., Gandelman, M., … Cassina, P.
692 (2012). Modulation of Astrocytic Mitochondrial Function by Dichloroacetate Improves
693 Survival and Motor Performance in Inherited Amyotrophic Lateral Sclerosis. *PLoS ONE*,
694 *7*(4), e34776. https://doi.org/10.1371/journal.pone.0034776

695 Nagai, M., Re, D. B., Nagata, T., Chalazonitis, A., Jessell, T. M., Wichterle, H., & Przedborski, S.
696 (2007). Astrocytes expressing ALS-linked mutated SOD1 release factors selectively toxic
697 to motor neurons. *Nature Neuroscience*, *10*(5), 615–622. https://doi.org/10.1038/nn1876

698 Olzmann, J. A., & Carvalho, P. (2019). Dynamics and functions of lipid droplets. *Nature Reviews*
699 *Molecular Cell Biology*, *20*(3), 137–155. https://doi.org/10.1038/s41580-018-0085-z

700 Paganoni, S., Macklin, E. A., Hendrix, S., Berry, J. D., Elliott, M. A., Maiser, S., … Cudkowicz, M.
701 E. (2020). Trial of Sodium Phenylbutyrate–Taurursodiol for Amyotrophic Lateral Sclerosis.
702 *New England Journal of Medicine*, *383*(10), 919–930.
703 https://doi.org/10.1056/NEJMoa1916945

Palamiuc, L., Schlagowski, A., Ngo, S. T., Vernay, A., Dirrig-Grosch, S., Henriques, A., … René, F. (2015). A metabolic switch toward lipid use in glycolytic muscle is an early pathologic event in a mouse model of amyotrophic lateral sclerosis. *EMBO Molecular Medicine*, *7*(5), 526–546. https://doi.org/10.15252/emmm.201404433

Patel, M. S., & Korotchkina, L. G. (2006). Regulation of the pyruvate dehydrogenase complex. *Biochemical Society Transactions*, *34*(2), 217. https://doi.org/10.1042/BST20060217

Patel, M. S., & Roche, T. E. (1990). Molecular biology and biochemistry of pyruvate dehydrogenase complexes 1. *The FASEB Journal*, *4*(14), 3224–3233. https://doi.org/10.1096/fasebj.4.14.2227213

Pellerin, L., & Magistretti, P. J. (2012). Sweet Sixteen for ANLS. *Journal of Cerebral Blood Flow & Metabolism*, *32*(7), 1152–1166. https://doi.org/10.1038/jcbfm.2011.149

Pharaoh, G., Sataranatarajan, K., Street, K., Hill, S., Gregston, J., Ahn, B., … Van Remmen, H. (2019). Metabolic and Stress Response Changes Precede Disease Onset in the Spinal Cord of Mutant SOD1 ALS Mice. *Frontiers in Neuroscience*, *13*(MAY), 487. https://doi.org/10.3389/fnins.2019.00487

Rahman, M. H., Bhusal, A., Kim, J.-H., Jha, M. K., Song, G. J., Go, Y., … Suk, K. (2020). Astrocytic pyruvate dehydrogenase kinase-2 is involved in hypothalamic inflammation in mouse models of diabetes. *Nature Communications*, *11*(1), 5906. https://doi.org/10.1038/s41467-020-19576-1

Renne, M. F., & Hariri, H. (2021). Lipid Droplet-Organelle Contact Sites as Hubs for Fatty Acid Metabolism, Trafficking, and Metabolic Channeling. *Frontiers in Cell and Developmental Biology*, *9*. https://doi.org/10.3389/fcell.2021.726261

Ryu, H., Smith, K., Camelo, S. I., Carreras, I., Lee, J., Iglesias, A. H., … Ferrante, R. J. (2005). Sodium phenylbutyrate prolongs survival and regulates expression of anti-apoptotic genes in transgenic amyotrophic lateral sclerosis mice. *Journal of Neurochemistry*, *93*(5), 1087–1098. https://doi.org/10.1111/j.1471-4159.2005.03077.x

Saneto, R., & De Vellis, J. (1987). Neuronal and glial cells: cell culture of the central nervous system. In A. Turner & H. Brachelard (Eds.), *Neurochemistry: a practical approach* (pp. 27–63). Oxford IRL Press.

Sauvanet, C., Duvezin-Caubet, S., di Rago, J.-P., & Rojo, M. (2010). Energetic requirements and bioenergetic modulation of mitochondrial morphology and dynamics. *Seminars in Cell & Developmental Biology*, *21*(6), 558–565. https://doi.org/10.1016/j.semcdb.2009.12.006

Smith, E. F., Shaw, P. J., & De Vos, K. J. (2019). The role of mitochondria in amyotrophic lateral sclerosis. *Neuroscience Letters*, *710*, 132933. https://doi.org/10.1016/j.neulet.2017.06.052

Smolič, T., Tavčar, P., Horvat, A., Černe, U., Halužan Vasle, A., Tratnjek, L., … Vardjan, N. (2021). Astrocytes in stress accumulate lipid droplets. *Glia*, (February), 1–23. https://doi.org/10.1002/glia.23978

742 Smolič, T., Zorec, R., & Vardjan, N. (2021). Pathophysiology of Lipid Droplets in Neuroglia.
743 *Antioxidants*, *11*(1), 22. https://doi.org/10.3390/antiox11010022

744 Stacpoole, P. W. (2017). Therapeutic Targeting of the Pyruvate Dehydrogenase
745 Complex/Pyruvate Dehydrogenase Kinase (PDC/PDK) Axis in Cancer. *JNCI: Journal of the*
746 *National Cancer Institute*, *109*(11), 1–14. https://doi.org/10.1093/jnci/djx071

747 Takubo, K., Nagamatsu, G., Kobayashi, C. I., Nakamura-Ishizu, A., Kobayashi, H., Ikeda, E., …
748 Suda, T. (2013). Regulation of Glycolysis by Pdk Functions as a Metabolic Checkpoint for
749 Cell Cycle Quiescence in Hematopoietic Stem Cells. *Cell Stem Cell*, *12*(1), 49–61.
750 https://doi.org/10.1016/j.stem.2012.10.011

751 Taylor, J. P., Brown, R. H., & Cleveland, D. W. (2016). Decoding ALS: From genes to mechanism.
752 *Nature*, *539*(7628), 197–206. https://doi.org/10.1038/nature20413

753 Valente, A. J., Maddalena, L. A., Robb, E. L., Moradi, F., & Stuart, J. A. (2017). A simple ImageJ
754 macro tool for analyzing mitochondrial network morphology in mammalian cell culture.
755 *Acta Histochemica*, *119*(3), 315–326. https://doi.org/10.1016/j.acthis.2017.03.001

756 Vargas, M. R., Pehar, M., Cassina, P., Beckman, J. S., & Barbeito, L. (2006). Increased
757 glutathione biosynthesis by Nrf2 activation in astrocytes prevents p75NTR-dependent
758 motor neuron apoptosis. *Journal of Neurochemistry*, *97*(3), 687–696.
759 https://doi.org/10.1111/j.1471-4159.2006.03742.x

760 Velebit, J., Horvat, A., Smolič, T., Prpar Mihevc, S., Rogelj, B., Zorec, R., & Vardjan, N. (2020).
761 Astrocytes with TDP-43 inclusions exhibit reduced noradrenergic cAMP and Ca2+
762 signaling and dysregulated cell metabolism. *Scientific Reports*, *10*(1), 6003.
763 https://doi.org/10.1038/s41598-020-62864-5

764 Zhang, W., Zhang, S.-L., Hu, X., & Tam, K. Y. (2015). Targeting Tumor Metabolism for Cancer
765 Treatment: Is Pyruvate Dehydrogenase Kinases (PDKs) a Viable Anticancer Target?
766 *International Journal of Biological Sciences*, *11*(12), 1390–1400.
767 https://doi.org/10.7150/ijbs.13325

768 Zhang, Y., Chen, K., Sloan, S. a, Bennett, M. L., Scholze, A. R., Keeffe, S. O., … Wu, X. J. Q.
769 (2014). An RNA-Sequencing Transcriptome and Splicing Database of Glia, Neurons, and
770 Vascular Cells of the Cerebral Cortex. *Journal of Neuroscience*, *34*(36), 11929–11947.
771 https://doi.org/10.1523/JNEUROSCI.1860-14.2014

772 Zhang, Y., Sloan, S. A., Clarke, L. E., Caneda, C., Plaza, C. A., Blumenthal, P. D., … Barres, B. A.
773 (2016). Purification and Characterization of Progenitor and Mature Human Astrocytes
774 Reveals Transcriptional and Functional Differences with Mouse. *Neuron*, *89*(1), 37–53.
775 https://doi.org/10.1016/J.NEURON.2015.11.013

776

777

780 # Figure Legends:

781

782 **Figure 1.** PDK2 siRNA treatment reduced PDK2 mRNA expression and PDK activity in
783 astrocytes. **A)** PDK2 relative mRNA expression in astrocytes treated with PDK2 siRNA, PDK1
784 siRNA, Negative control siRNA (NC siRNA), and control astrocytes, quantified by qPCR. **B)**
785 Relative levels of phosphorylated PDH and total PDH in cultured astrocytes. Top pane:
786 Representative western blot using antibodies against phosphorylated PDH (PDH PSer293),
787 total PDH E1α, and α-tubulin as loading control of protein samples of astrocytes treated with
788 PDK2 siRNA, PDK1 siRNA, Negative control siRNA (NC siRNA) of vehicle. Bottom pane:
789 Phosphorylated PDH/total PDH ratio quantification. **C) PDK4 relative mRNA expression in**
790 **astrocytes treated with PDK2 siRNA, NC siRNA, or in control astrocytes.** All data are
791 presented as mean ± SEM from 4-5 independent experiments. *p<0.05, ****p<.01, ***p<.001.**

792

793 **Figure 2**. PDK2 knockdown improves the mitochondrial function of SOD1G93A-expressing
794 astrocytes. **A)** Representative slope curves of the oxygen consumption rate (OCR) for non-Tg
795 and SOD1G93A astrocytes (control and treated with PDK2 siRNA or DCA over time. Arrows
796 indicate the time of addition of oligomycin, FCCP, and rotenone + antimycin A. **B)** Respiratory
797 parameters (basal respiration, **proton leak respiration**, respiration linked to ATP production,
798 maximal, and non-mitochondrial respiration) obtained from the OCR profiles of the different
799 treatment groups. Data are expressed as % of non-Tg control. **C)** Spare respiratory capacity,
800 Coupling efficiency, and Cell respiratory control ratio (RCR) of the same treatment groups. All
801 data are presented as mean ± SEM from 3 independent experiments. *p <.05, **p<.01,
802 ***p<.001.

803

804 **Figure 3.** Effects of PDK2 silencing on SOD1G93A-expressing astrocyte mitochondrial network
805 structure. **A)** Representative images of mitotracker green-labeled non-Tg or SOD1G93A
806 astrocyte mitochondria in control conditions or treated with negative control siRNA (NC
807 siRNA), PDK2 siRNA, or DCA. Scale bar: 10 µm. **B)** Mitochondrial network morphological
808 parameters: mean mitochondrial length, mean mitochondrial rod/branch length, and
809 percentage of mitochondria forming networks (3 or more branches), obtained from the
810 different treatment groups. All data are presented as mean ± SEM from 4 experiments. *p
811 <.05, **p<.01, ***p<.001.

812

813 **Figure 4.** PDK2 knockdown alters lipid droplet accumulation in SOD1G93A astrocytes. **A)**
814 Representative images from non-Tg or SOD1G93A astrocyte monolayers treated as indicated,
815 stained with Oil Red O to label LD (red), and processed for GFAP immunofluorescence (green)
816 and DAPI for nuclei labeling (blue). Scale bar: 20 µm. **B)** Quantification of the mean number of
817 Oil Red O-stained structures per cell in the indicated groups. All data are presented as mean ±
818 SEM from 3 independent experiments. *p<.05.

819

820 **Figure 5.** PDK2 knockdown recovers the ability of SOD1G93A astrocytes to support MN
821 survival. **A)** Representative image of an astrocyte-motor neuron co-culture processed for βIII-
822 tubulin immunocytochemistry for motor neuron survival quantification. Scale bar: 100 µm. **B)**
823 non-Tg motor neuron survival on top of non-Tg or SOD1G93A astrocyte monolayers following
824 incubation with PDK2 siRNA, negative control (NC) siRNA, or DCA. Data are presented as the
825 percentage of MN survival on top of a non-Tg astrocyte monolayer (control). All data are
826 presented as mean ± SEM from 3 experiments. *p <.05, **p<.01, ***p<.001.

GLIA

A

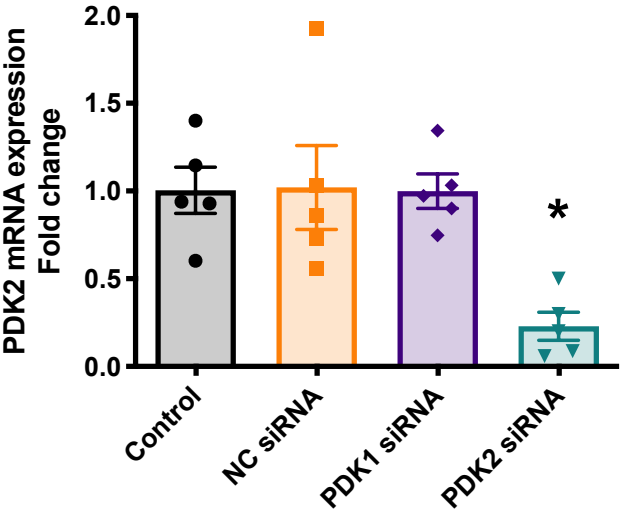

B

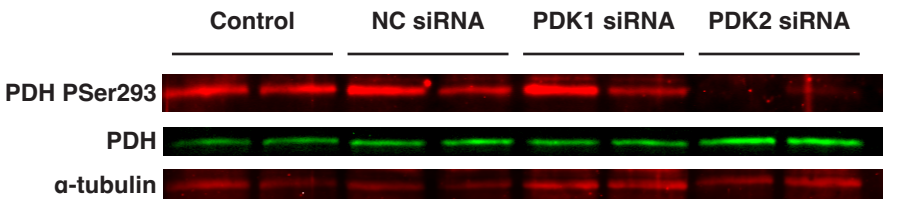

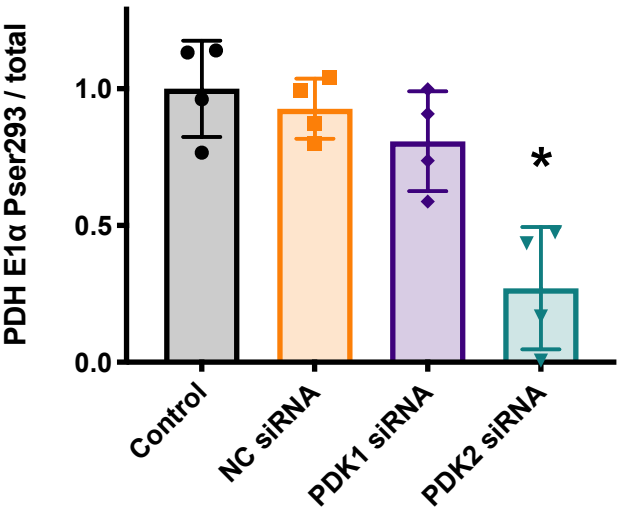

C

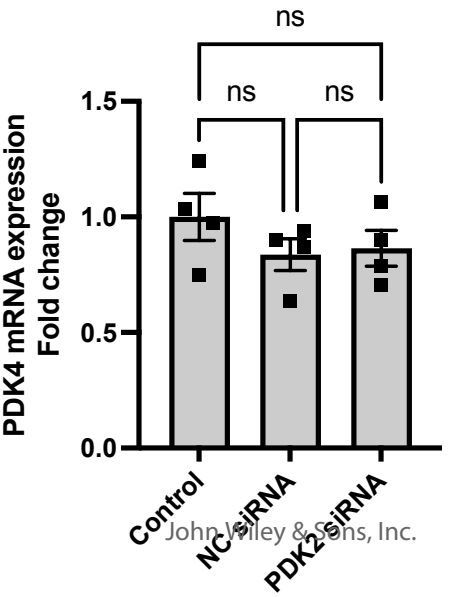

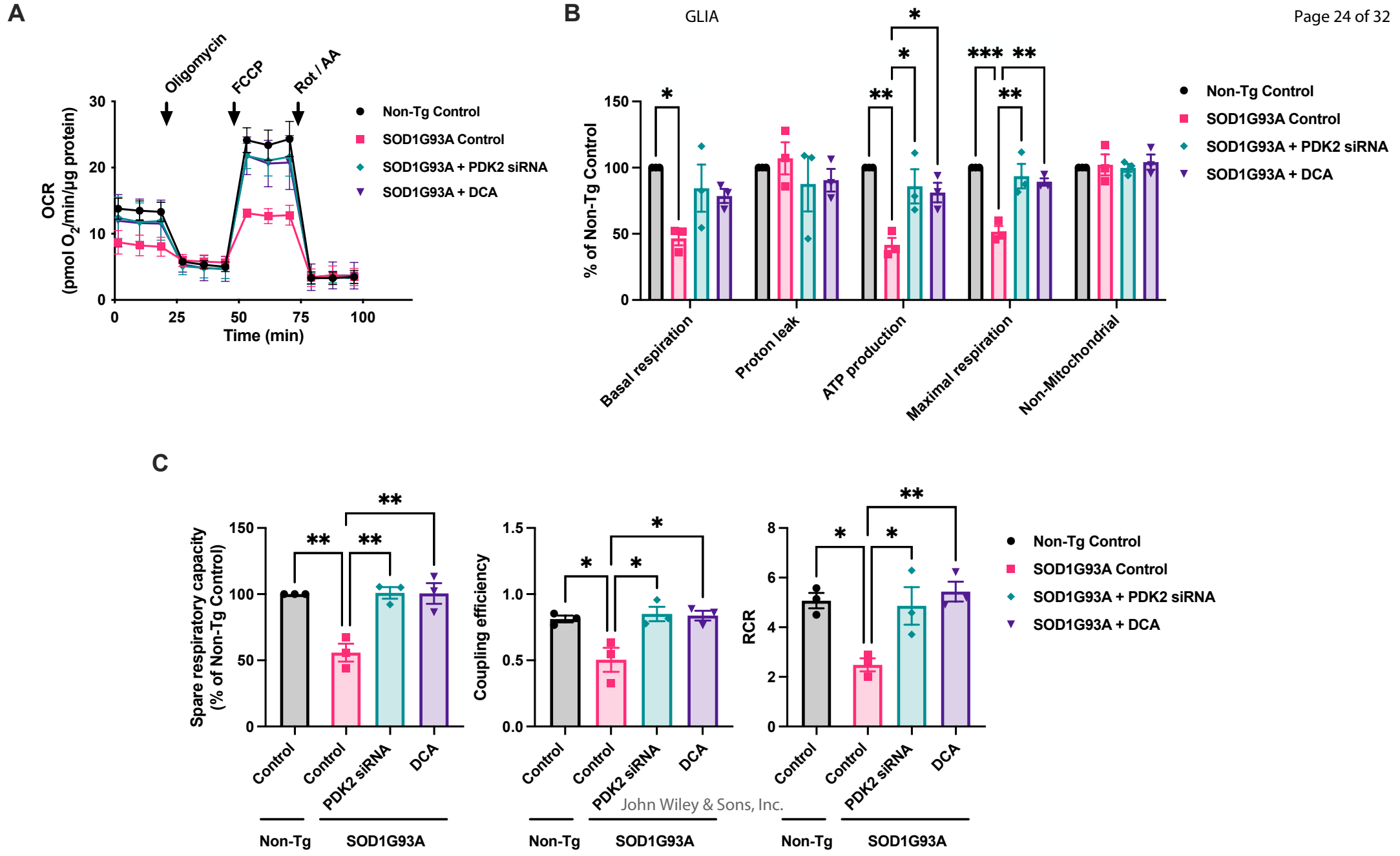

A

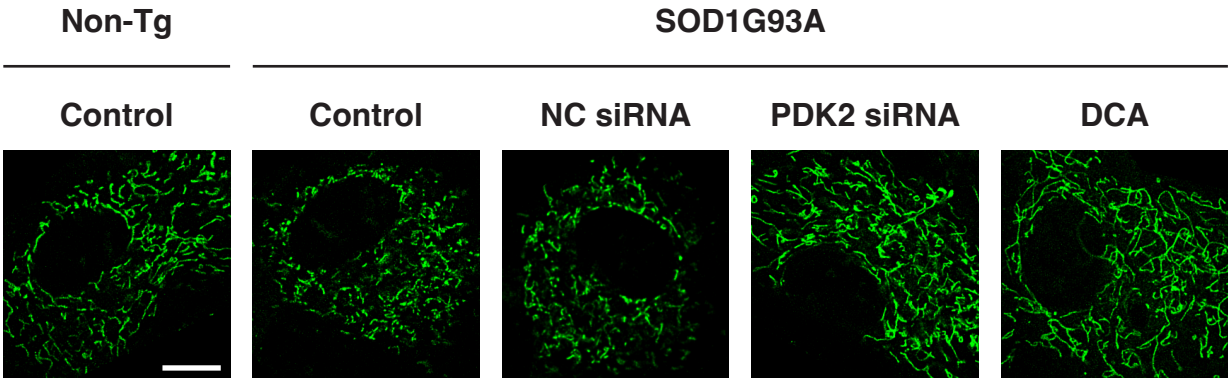

B

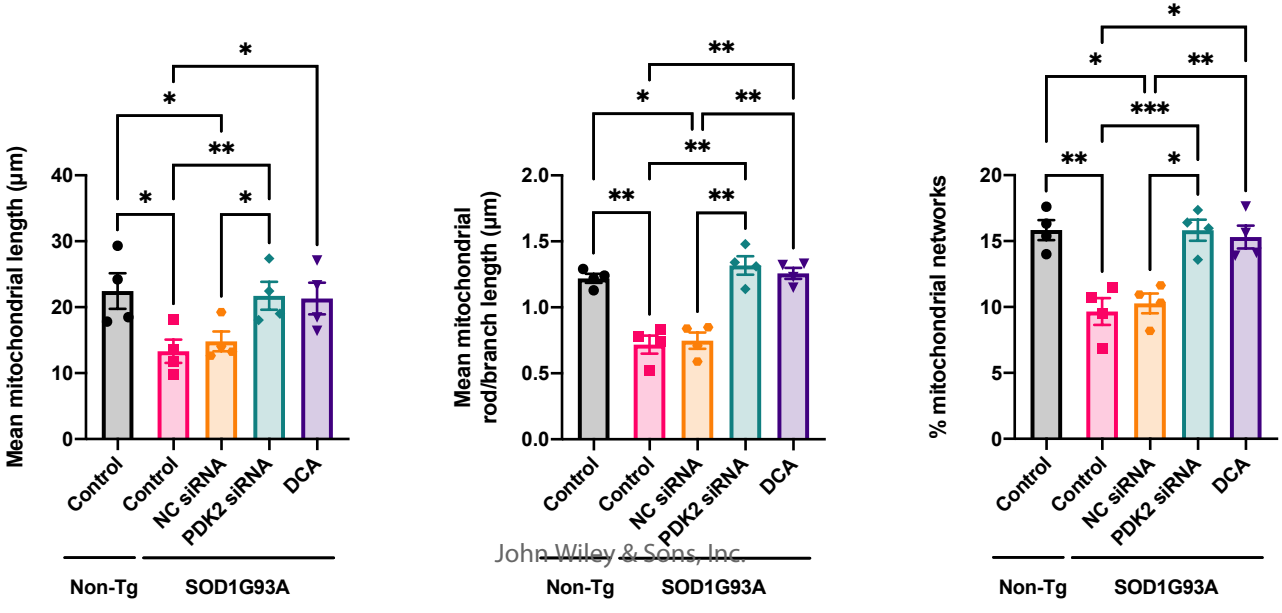

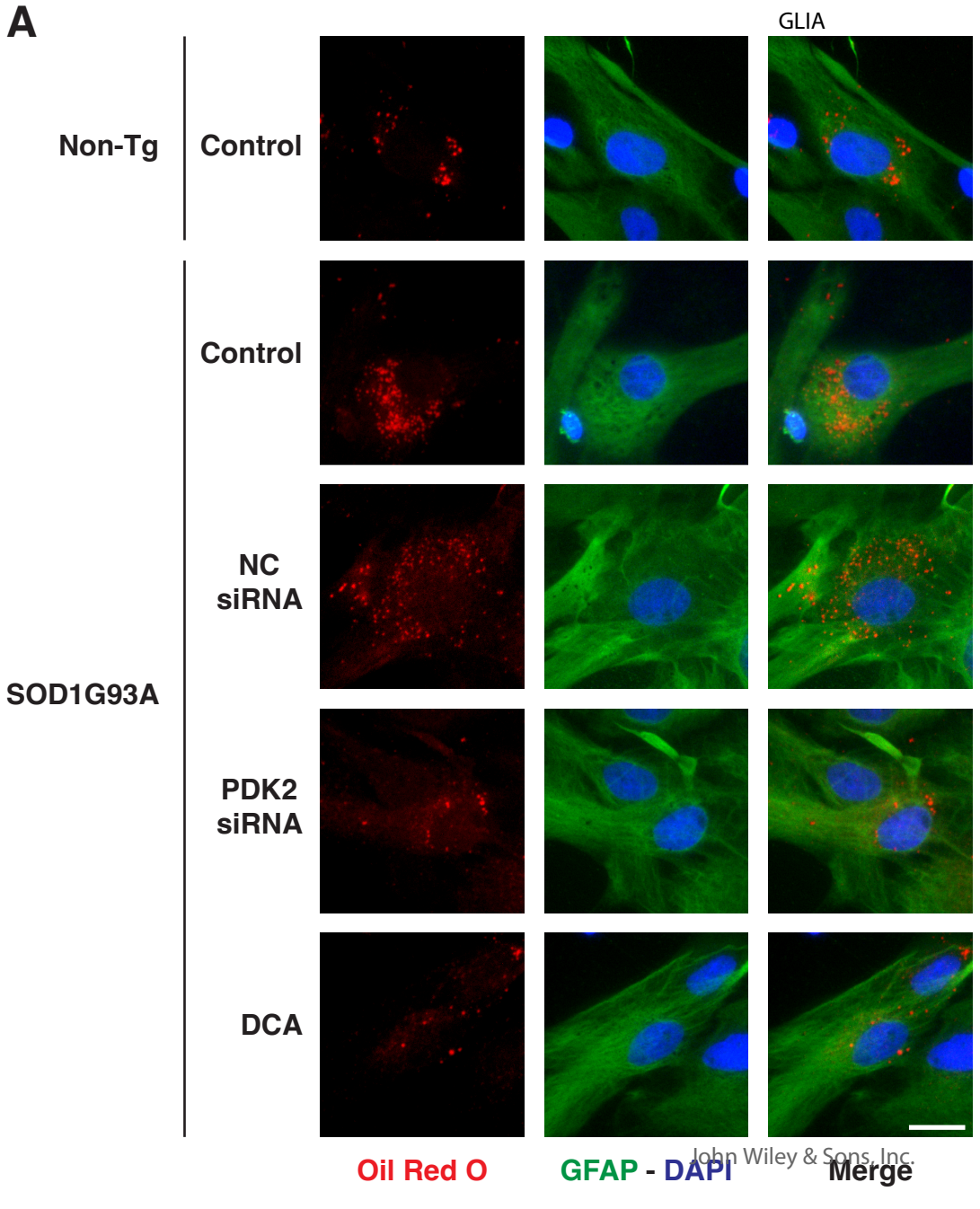

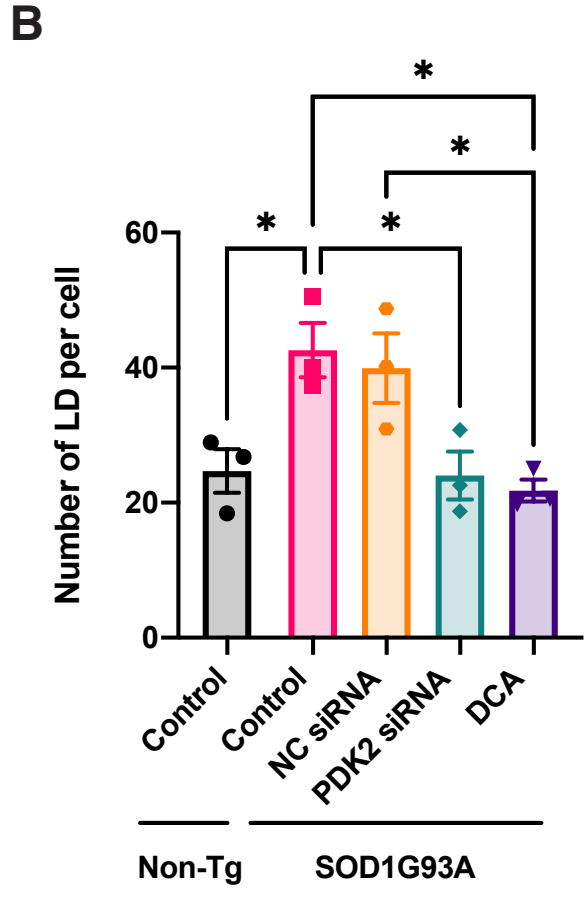

A

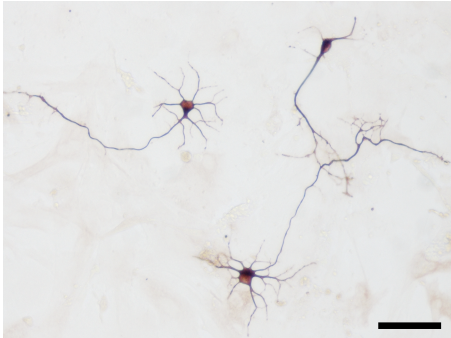

B